Eur. Phys. J. Appl. Phys. **92**, 10905 (2020)

https://doi.org/10.1051/epjap/2020200020

THE EUROPEAN PHYSICAL JOURNAL APPLIED PHYSICS

Regular Article

Modeling the dynamic behavior of laminated steels using a Fourier-based approach★

Reza Zeinali*, Dave Krop and Elena Lomonova

Eindhoven University of Technology, 5612 AZ Eindhoven, The Netherlands

Received: 28 January 2020 / Received in final form: 21 April 2020 / Accepted: 8 September 2020

Abstract. A new magneto-dynamic model is proposed to approximate the dynamic hysteresis effect in laminated steels considering the static hysteresis, eddy-current field, and excess field. An accurate congruency-based hysteresis model is used to predict the static hysteresis field. The eddy-current is determined from the 1D diffusion equation and the well-known Bertotti empirical equation is utilized to model the excess-field effect. The dynamic lamination model obtained from coupling three field components is solved using a Fourier-based approach. In this approach, the flux density across the lamination thickness is approximated by a cosine-based Fourier series. The coefficients of the Fourier series are determined by solving a system of nonlinear equations through an iterative procedure. Owing to the employed congruency-based static hysteresis model, the proposed magneto-dynamic model offers high accuracy for arbitrary magnetization regimes. To validate the model accuracy, the model results are compared with sinusoidal and multi-harmonic measurements. The comparison shows that the proposed model predicts the dynamic hysteresis phenomenon in laminated steels with a relative energy error of less than 7%.

1 Introduction

Due to rising energy costs, high-efficiency motors have been increasingly in demand in the last decade. Furthermore, for reasons of compactness and thus weight, high-speed machines are preferred. Designing a high-speed high-efficiency electrical drive relies on accurate iron loss calculations in ferromagnetic laminated steels. Empirical models like Bertotti and Steinmetz are commonly used in Finite Element Method (FEM)-based software for iron loss calculation [1]. The FEM simulation results obtained by a non-hysteretic B–H are post-processed by the empirical equations to determine iron losses. However, approximating the actual magnetization behavior by a single-valued non-hysteretic B-H curve results in an erroneous calculation of the flux density and iron losses [2,3]. In order to avoid such a miscalculation, the actual behavior of magnetic material has to be taken into account in FE simulations. The magnetic behavior of ferromagnetic materials operating under varying magnetic flux depends on several interconnected phenomena including, hysteresis, excess field, and eddy current.

The hysteresis phenomenon is referred to as the static component of the magnetic field. Various static hysteresis models are proposed in the literature. The static Preisach model is one of the phenomenological hysteresis models which has been thoroughly investigated in the literature [4–8]. In [9], several commonly used hysteresis models including Jiles–Atherton (J–A), GRUCAD, Stop, Tellinen (TLN), and Z-M hysteresis models are studied and compared in terms of identification procedure facilities, accuracy, numerical implementation, and computational effort. A congruency-based static hysteresis model is proposed in [10]. In this model, any second or higher-order reversal curve is approximated using internal segments of the First Order Reversal Curves (FORCs). In [11], the congruency-based hysteresis model proposed in [10] is extended and a Second-order Congruency-based Model (SCM) is introduced. In the SCM, in addition to the FORCs, Second-Order Reversal Curves (SORCs) are included in the model to achieve higher accuracy. The accuracy of the SCM is validated by comparing the model results to quasi-static measurements with arbitrary wave-shapes.

The excess-field and eddy-current phenomena are referred to as dynamic components of the magnetic field. Those components are produced when a time varying magnetic field is applied to the magnetic material. The excess-field effect is created because of the viscous property of the domain walls in magnetic materials. As a result, there is always a time delay between the local flux density and the local field strength. Since the physical process of the domain wall movement is not well understood yet, the excess-field effect is modeled using engineering phenomenology. The excess-field effect is considered in the dynamic model using

$$H_{ex}(x,t) = k_{ex}\left|\frac{\partial B_z(x,t)}{\partial t}\right|^{\alpha-1}\frac{\partial B_z(x,t)}{\partial t}, \qquad (1)$$

★Contribution to the Topical Issue "International Symposium on Electromagnetic Fields in Mechatronics, Electrical and Electronic Engineering (ISEF 2019)", edited by Adel Razek.

* e-mail: r.zeinali@tue.nl

where k_{ex} and α are obtained by fitting the modeled dynamic loops to measurements.

According to Faraday's law, when a magnetic material is exposed to a varying magnetic flux, eddy currents are induced, due to the conductivity of the material. The induced eddy currents create a magnetic field opposing the change of the magnetic flux density. This behavior is described by the so-called diffusion equation. Owing to the thin long dimensions of steel lamination, edge effects can be neglected, and the diffusion equation is then simplified into a 1D spatial partial differential equation (PDE) given by

$$\frac{\partial^2 H_z(x,t)}{\partial x^2} = \sigma \frac{\partial B_z(x,t)}{\partial t}, \tag{2}$$

where

$$H_z(x,t) = H_{hy}(x,t) + H_{ex}(x,t), \tag{3}$$

σ is the material conductivity and $H_{hy}(x,t)$ is the hysteresis component of the magnetic field [4].

Based on the loss separation theory proposed by Bertotti [1], the relationship between the magnetic field components is expressed by

$$H_z(x,t) = H_{in}(t) - H_{eddy}(x,t), \tag{4}$$

where $H_{in}(t)$ is the external field applied to the magnetic material.

In the classical eddy-current approach, it is assumed that the magnetic field strength, H_z, is homogeneous across the material thickness [1]. As a result, the simplified eddy-current field is obtained by

$$H_{eddy}(t) = \sigma \frac{d^2}{12} \frac{\partial B_z(t)}{\partial t}. \tag{5}$$

The classical eddy-current approach is simple and computationally efficient, however the skin effect is neglected, and this results in a wrong prediction of the eddy-current field, especially at higher frequencies. Figure 1 illustrates an example of a non-homogeneous flux density and magnetic field strength across laminated steel with a thickness of d.

In order to avoid the error introduced by the classical eddy-current simplification, a more accurate solution of the diffusion equation is required. Several approaches like analytic techniques [12], Finite Difference (FD) [13], Magnetic Equivalent Circuit (MEC) [14], Parametric Magneto Dynamic (PMD) [15,16], Diffusion equation mean frequency (DEMF) [17], and Mesh Free (MF) methods [18,19] have been proposed in literature to solve the 1D diffusion equation for a thin steel lamination. In this study, the MF approach is used. In the MF approach. The flux density across the lamination thickness is approximated by a cosine-based Fourier series. The coefficients of the Fourier series are obtained by satisfying the weak formulation of the governing PDE.

In this study, a dynamic magnetic model is proposed for non-oriented laminated steels. The static hysteresis component is modeled by the SCM proposed in [11].

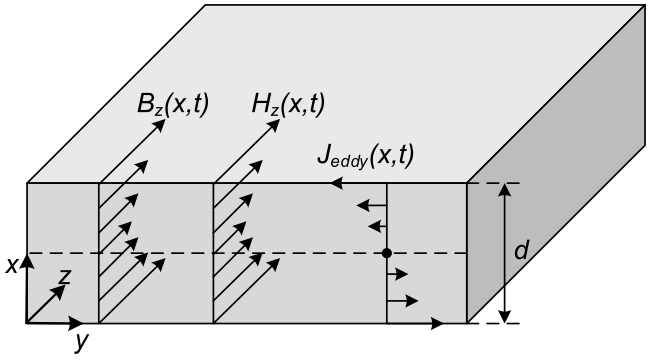

Fig. 1. Illustration of the non-homogeneous magnetic field across the thickness of laminated steel.

The static hysteresis and excess-field components are coupled with the diffusion equation, and the MF approach is applied to solve the resulting equation. This paper is organized as follows, the SCM is discussed in Section 2. In Section 3, the MF approach is explained and applied to the dynamic lamination equation. In Section 4, the model results are compared with measurements. Finally, the obtained results are discussed, and conclusions are made in Section 5.

2 Second-order congruency-based static hysteresis model

Accuracy of the dynamic hysteresis model is highly dependent on the static hysteresis model. Therefore, an accurate dynamic lamination model needs an accurate static hysteresis model. In [10], a type of congruency-based model is proposed, which uses a set of a FORCs to approximate second or higher-order reversal curves. To this end, a congruency regularity is defined to choose the proper transplant of FORCs for approximating second or higher-order reversal curves. According to this congruency regularity, any second or higher-order reversal curve with specific ΔB and ΔH is obtained by a weighted sum of H-congruent and B-congruent FORC transplants. The weight factor is determined based on the magnetic history of the material.

In [11], the congruency hysteresis model in [10] is extended to achieve higher accuracy. In the extended model, so-called SCM, both measured FORCs and second-order reversal curves (SORCs) are employed to approximate third or higher-order reversal curves. To this end, a congruency regularity is proposed for determining third or higher reversal curves based on the measured FORCs and SORCs. According to this congruency regularity, any third or higher-order reversal curve is congruent to a SORC with the same reversal point.

The idea behind the proposed regularity is graphically clarified in Figures 2 and 3. Figure 2 illustrates a set of measured reversal curves up to a third-order reversal curve (TORC) for NO27 magnetic material. To obtain the same reversal curves by means of the SCM, it is obvious that the major loop, the FORC, and the SORC are directly attainable from the performed measurements, however,

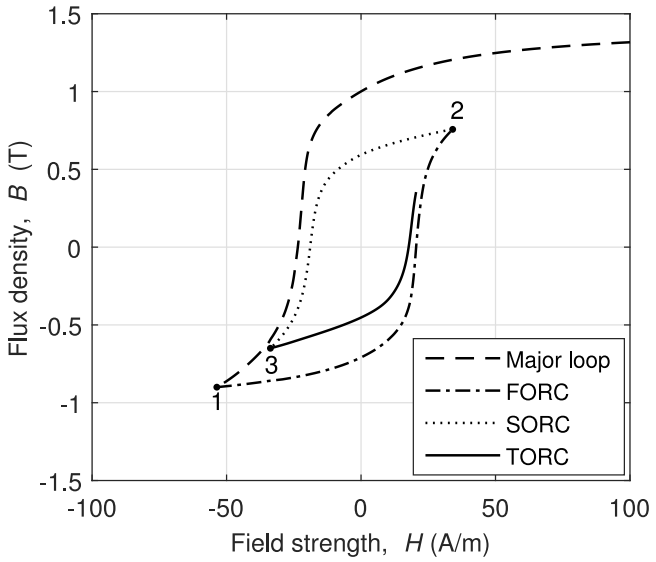

Fig. 2. Reversal curves for NO27 magnetic material up to a TORC.

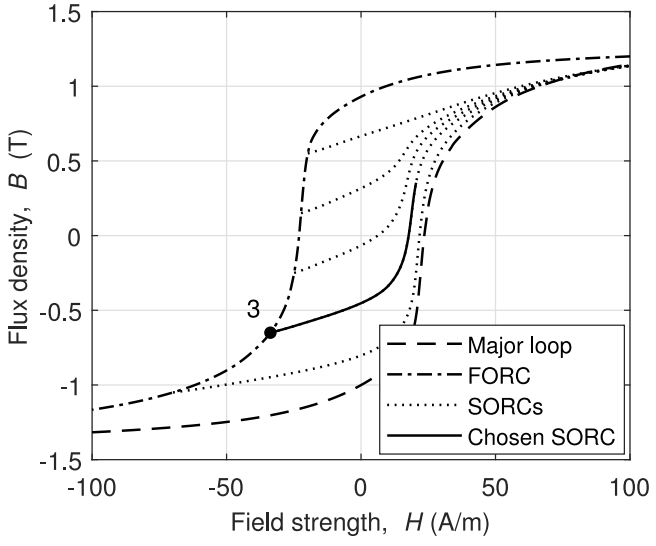

Fig. 3. Illustration of the proposed regularity for choosing a proper SORC for approximating the TORC shown in Figure 2.

the TORC needs to be approximated by a properly chosen SORC based on the proposed congruency regularity. As seen in Figure 2, point 3 is the reversal point of the TORC. Hence, the TORC is congruent to a SORC which has the reversal point starting from point 3. It is obvious that the reversal point of the SORCs is located on the FORCs. Since the FORCs do not intersect each other, there is only one FORC passing through a specific reversal point. The FORC passing through reversal point 3 is shown in Figure 3. All the SORCs reversing from the obtained FORC are available from the measurements and the proper one reversing from point 3 is chosen to approximate the target TORC shown in Figure 2.

In order to validate the accuracy and effectiveness of the SCM, the model results are compared to the experimental data for arbitrarily measured reversal curves up to and including the eighth order as shown in Figure 4. As seen in the figure, there is a good correlation between the model and the measured data, which proves that the model is capable of predicting arbitrary B–H curves. The relative error in dissipated energy is less than 1% between the model results and the measurement shown in Figure 4. Furthermore, it is possible to implement this model as a function of either B or H. In Section 3, it is shown that B-input implementation of the static model, i.e. $H(B)$, is preferred, as it makes the dynamic lamination model more computationally efficient.

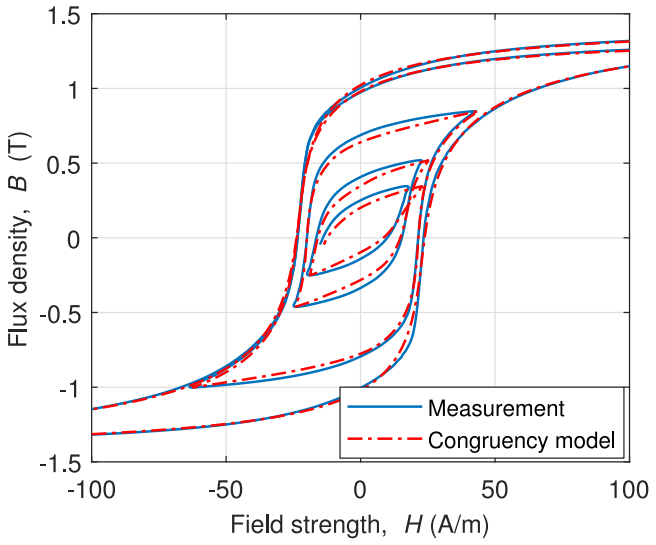

Fig. 4. Comparison of the SCM with quasi-static reversal curve measurement up to and including the 8th order reversal curve.

3 Dynamic lamination model

In this section, the solution of the dynamic lamination model expressed by (2), (3), and (4) is presented. The Mesh-Free (MF) approach proposed in [19] is utilized to solve the model. The excess field component is obtained from (1) as a function of the flux density B_z. If the hysteresis component is available as a function of B_z, the dynamic lamination model can be solved considering the flux density as the unknown. Therefore, it is preferred to implement the SCM as a function of flux density B_z, i.e. $H_{hy}(B_z)$.

In the MF approach, a cosine-based Fourier series, expressed by (6) and (7), is used to approximate the flux density across the lamination thickness, i.e. $x \in [-d/2, d/2]$. So

$$B_z(x,t) = \sum_{n=0}^{N_h-1} b_n(t)\,\alpha_n(x), \tag{6}$$

where

$$\alpha_n(x) = \cos\left(2n\pi\frac{x}{d}\right). \tag{7}$$

By substituting (6) into (2), performing a double integration with respect to x, and applying (4) as a

boundary condition, the field strength, H_z, is obtained by

$$H_z(x,t) = H_{in}(t) - \sigma\left[\frac{\partial b_0}{\partial t}\left(\frac{d^2}{8} - \frac{x^2}{2}\right) + \sum_{n=1}^{N_h-1}\frac{\partial b_n}{\partial t}\left(\frac{d}{2n\pi}\right)^2\beta_n(x)\right], \quad (8)$$

where

$$\beta_n(x) = \cos\left(2n\pi\frac{x}{d}\right) - \cos(n\pi). \quad (9)$$

All field components in (4) are available as functions of the flux density. Equation (4) is a nonlinear equation in time and 1D space and it cannot be solved analytically, so it is set to be weakly satisfied. By multiplying (4) with the basis functions, $\alpha_n(x)$, and subsequently integrating the obtained equation over the lamination thickness, the weakly-satisfied form of (4) is obtained as

$$\begin{bmatrix} H_{in}(t) \\ 0 \\ \vdots \end{bmatrix} = \frac{1}{d}\int_{-\frac{d}{2}}^{\frac{d}{2}} H_z(x,t)\begin{bmatrix} \alpha_0(x) \\ \alpha_1(x) \\ \vdots \end{bmatrix} dx + \sigma\mathbf{C}\frac{\partial}{\partial t}\begin{bmatrix} b_0(t) \\ b_1(t) \\ \vdots \end{bmatrix}, \quad (10)$$

where

$$H_z(x,t) = H_{hy}(x,t) + H_{ex}(x,t). \quad (11)$$

The constant $\mathbf{C}$ in (10) is a square matrix for which the nonzero elements are obtained by evaluating the following four integrals for $n = 1, \ldots, N_h - 1$ analytically

$$C_{00} = \frac{1}{d}\int_{-\frac{d}{2}}^{\frac{d}{2}}\left(\frac{d^2}{8} - \frac{x^2}{2}\right)dx, \quad (12)$$

$$C_{n0} = \frac{1}{d}\int_{-\frac{d}{2}}^{\frac{d}{2}}\left(\frac{d^2}{8} - \frac{x^2}{2}\right)\cos\left(2n\pi\frac{x}{d}\right)dx, \quad (13)$$

$$C_{0n} = -\frac{1}{d}\int_{-\frac{d}{2}}^{\frac{d}{2}}\left(\frac{d}{2n\pi}\right)^2\cos(n\pi)\,dx, \quad (14)$$

$$C_{nn} = \frac{1}{d}\int_{-\frac{d}{2}}^{\frac{d}{2}}\left(\frac{d}{2n\pi}\right)^2\cos^2\left(2n\pi\frac{x}{d}\right)dx. \quad (15)$$

Since the hysteresis field and the excess-field components are nonlinear functions of the flux density, the integral in (10) cannot be solved analytically. However, it can be evaluated semi-analytically by sampling the field strength term, $H_z(x,t)$, over the lamination thickness at N_s points for a given flux density and applying the fast cosine transform (FCT) to the sampled points of the field strength as follows

$$H_z(x,t) = \sum_{n=0}^{N_s-1} h_n(t)\,\alpha_n(x). \quad (16)$$

Using the obtained FCT coefficients, the integral in (10) is evaluated next,

$$\frac{1}{d}\int_{-\frac{d}{2}}^{\frac{d}{2}} H_z(x,t)\begin{bmatrix} \alpha_0(x) \\ \alpha_1(x) \\ \vdots \end{bmatrix} dx = \frac{1}{2}\begin{bmatrix} 2h_0(t) \\ h_1(t) \\ \vdots \end{bmatrix}. \quad (17)$$

By substituting (17) into (10) and applying the backward Euler method for time discretization, the following system of nonlinear equations is obtained

$$\begin{bmatrix} H_{in}(t_i) \\ 0 \\ \vdots \end{bmatrix} = \frac{1}{2}\begin{bmatrix} 2h_0(t_i) \\ h_1(t_i) \\ \vdots \end{bmatrix} + \frac{\sigma}{\Delta t}\mathbf{C}\left(\begin{bmatrix} b_0(t_i) \\ b_1(t_i) \\ \vdots \end{bmatrix} - \begin{bmatrix} b_0(t_{i-1}) \\ b_1(t_{i-1}) \\ \vdots \end{bmatrix}\right), \quad (18)$$

where Δt is the time-step length.

Equation (18) is a system of nonlinear equations which is solved iteratively via the Newton-Raphson (NR) method. The NR method makes use of the Jacobian matrix to perform iterative steps. The elements of this Jacobian matrix are

$$J_{mn} = \frac{1}{d}\int_{-\frac{d}{2}}^{\frac{d}{2}}\frac{\partial H_z}{\partial B_z}\alpha_m(x)\,\alpha_n(x)\,dx + \frac{\sigma}{\Delta t}C_{mn}, \quad (19)$$

where the differential reluctivity, $\partial H_z/\partial B_z$, has two components as given in (20). One component comes from the hysteresis field and the other component is due to the excess field.

$$\frac{\partial H_z}{\partial B_z} = \frac{\partial H_{hy}}{\partial B_z} + \frac{\partial H_{ex}}{\partial B_z}. \quad (20)$$

The hysteresis field reluctivity is obtained using the proposed static hysteresis model and the excess-field reluctivity is expressed analytically by

$$\frac{\partial H_{ex}}{\partial B_z} = \alpha\frac{k_{ex}}{\Delta t}\left|\frac{B_z(x,t_i) - B_z(x,t_{i-1})}{\Delta t}\right|^{\alpha-1}. \quad (21)$$

The integral term in (19) is evaluated in a similar semi-analytic way as the integral in (17). First, the differential reluctivity is sampled across the lamination thickness and the FCT is applied so as to determine the coefficients of the cosine series. Finally, the integral is solved analytically for the resulting triple cosine product.

The resultant nonlinear system of equations expressed by (18) can be solved for either $H_{in}(t)$, applied external

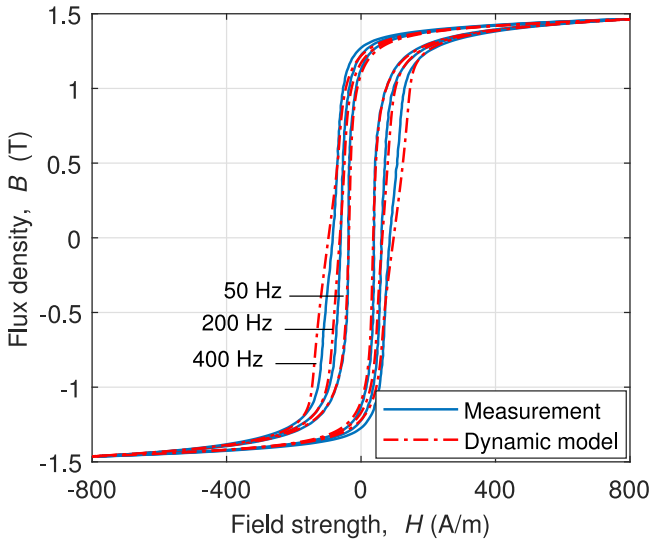

Fig. 5. Comparison of the proposed dynamic model results with the B-sinusoidal measurements for the obtained optimal excess-field parameters.

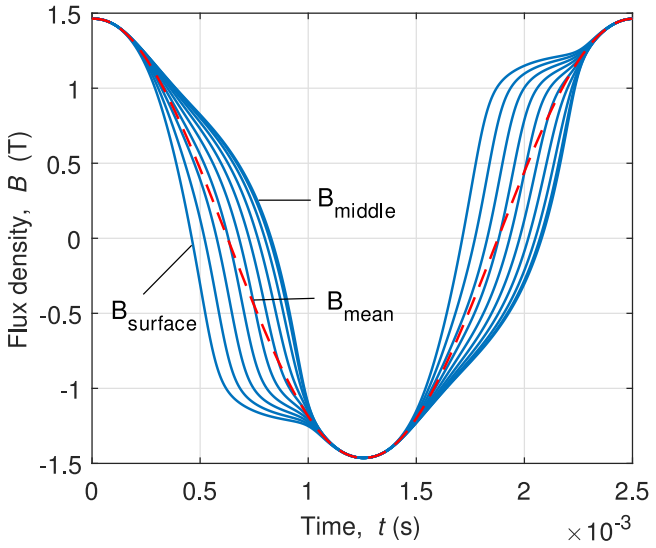

Fig. 6. The nodal and mean flux density waveforms for the nodal points at locations ranging from the surface to the middle of the lamination sheet with maximum mean-flux-density of 1.45 T.

field, or $b_0(t)$, mean flux density across the lamination thickness, as the input parameter. The presented results in Section 4 are obtained by imposing $b_0(t)$ as the input parameter. To this end, the equation in the first row of (18) is excluded from the system of equations. The same exclusion is applied to the Jacobian matrix, as well. Then, the rest of the system of equations is solved to obtain $b_1(t)$, $b_2(t)$, ..., and $b_{N_h-1}(t)$. Finally, the equation in the first row of (18) is evaluated separately to obtain $H_{in}(t)$ for an imposed $b_0(t)$ as follows:

$$H_{in}(t) = h_0(t) + \frac{\sigma}{\Delta t}\sum_{n=0}^{N_h-1} C_{0n} b_n(t). \qquad (22)$$

4 Dynamic model results

In this section, the accuracy of the proposed dynamic lamination model is validated for different sinusoidal and arbitrary AC measurements of NO27 magnetic material. First, the parameters of the excess field, k_{ex}, and α need to be identified. For this purpose, the dissipated energy error between the model and measured major B-sinusoidal loops at five different frequencies, i.e. 50, 100, 200, 300, and 400 Hz is minimized through an optimization procedure. The optimal values obtained for k_{ex}, and α as the result of the applied optimization are 0.184 and 0.57, respectively. Figure 5 compares the optimized dynamic model results with the measured B-sinusoidal loops for three frequencies of 50, 200, and 400 Hz. The relative dissipated energy errors between the model results and the measurements are 4.1%, 1.8%, and 2.8% for the 50, 200, and 400 Hz loops, respectively. The discrepancies happen due to the 2-coefficient empirical equation used to model the excess field. To increase the dynamic model accuracy, one may utilize a more elaborate excess field with a higher number of coefficients [13].

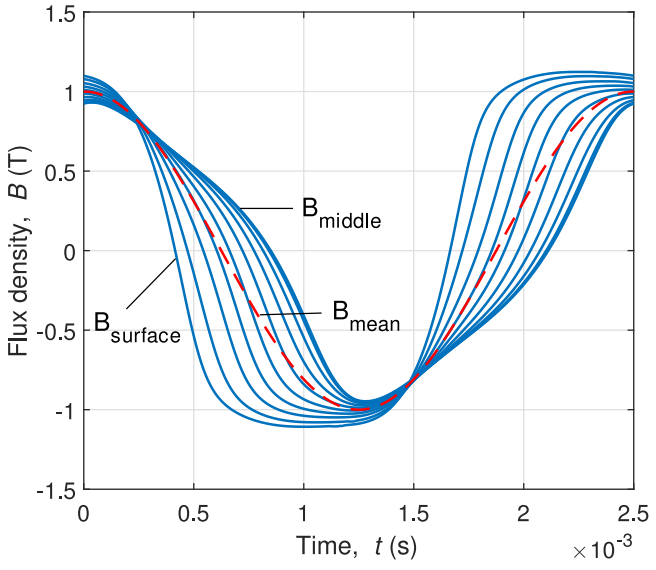

Fig. 7. The nodal and mean flux density waveforms for the nodal points at locations ranging from the surface to the middle of the lamination sheet with maximum mean-flux-density of 1 T.

Figures 6 and 7 show the flux density distribution across the lamination thickness for 400 Hz B-sinusoidal excitation with maximum flux density values of 1.45 and 1 T, respectively. The solid lines in the figures illustrate ten nodal flux density waveforms (at locations ranging from the surface to the middle of the lamination sheet), and the dashed line depicts the mean flux density waveform. As seen in Figure 6, since the material is rather saturated, the maximum flux density happens almost at the same time instant for all nodal points across the lamination thickness. However, this is not the case in Figure 7 where maximum flux density is 1 T. The results presented in Figures 6 and 7 reveal that the flux density is a

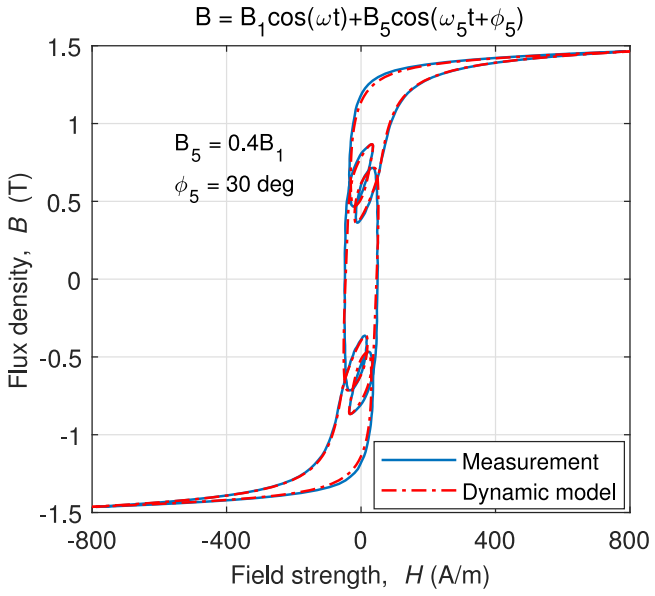

Fig. 8. Comparison of the proposed dynamic model with measurements in which the flux density contains the fundamental component + 5th harmonic.

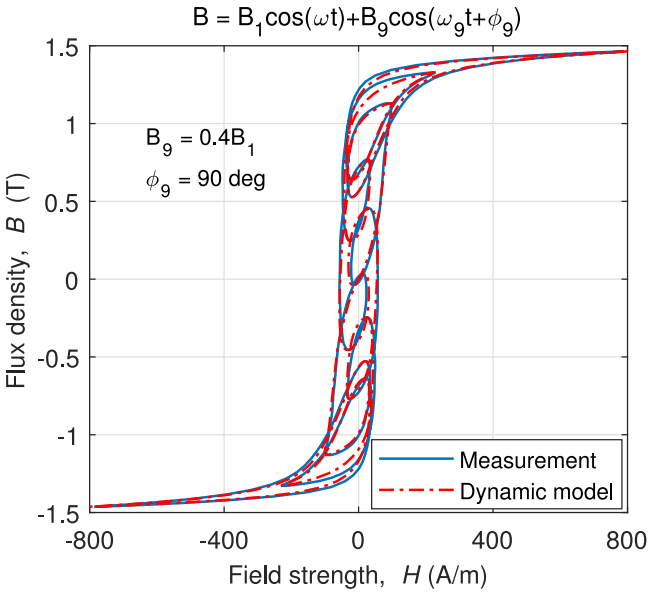

Fig. 10. Comparison of the proposed dynamic model with measurements in which the flux density contains the fundamental component + 9th harmonic.

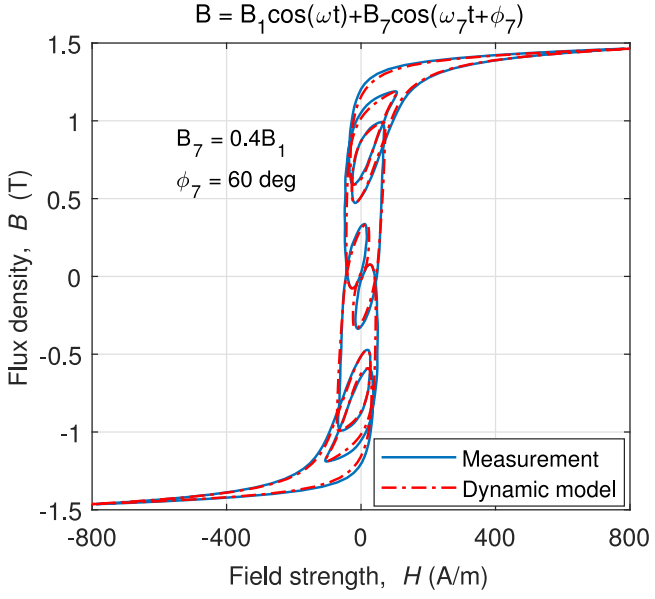

Fig. 9. Comparison of the proposed dynamic model with measurements in which the flux density contains the fundamental component + 7th harmonic.

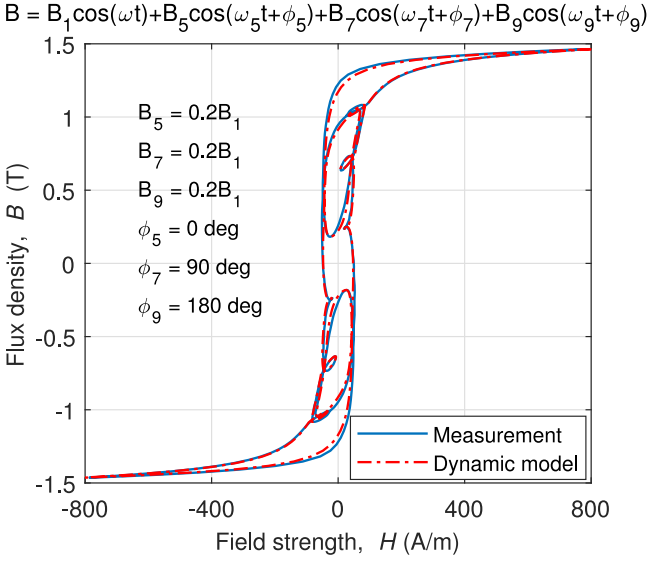

Fig. 11. Comparison of the proposed dynamic model with measurements in which the flux density contains the fundamental component, + 5th harmonic, + 7th harmonic, and + 9th harmonic.

function of both time and position and the classical eddy-current approach is a rough approximation of the diffusion equation, especially at higher frequencies. Therefore, it is necessary to have a more accurate solution of the diffusion equation considering skin-effect to obtain an accurate dynamic lamination model.

The results shown in Figure 5 indicate that the proposed dynamic lamination model is able to accurately model the magnetic field and iron losses in the magnetic material when the flux density is sinusoidal. However, the flux density of the steel lamination in electrical machines is not necessarily a pure sinus wave and it may contain higher-order harmonics. Therefore, it is crucial to investigate the model performance for the flux density waveforms containing higher harmonics. To this end, the model results are compared with the experimental data, in which the flux density waveform contains the fundamental component at 50 Hz plus a single higher harmonic, i.e. 5th, 7th or 9th harmonic, in Figures 8, 9, and 10, respectively. The relative dissipated energy-error for the 5th, 7th, and 9th harmonic cases is 5.8%, 6%, and 6.8%, respectively. Figure 11 validates the model performance

for a multi-harmonic case in which the flux density waveform is composed of the fundamental component at 50 Hz plus 5th, 7th, and 9th harmonics. The relative dissipated energy error is 5.2% in this case.

5 Conclusion

In this paper, a magneto-dynamic model for laminated steels has been presented. An accurate congruency-based model has been used to approximate the static hysteresis component of the magnetic field. In this static hysteresis model, the measured FORCs and SORCs have been employed to obtain the third or higher-order reversal curves. Instead of the classical eddy-current approach, the mesh-free (MF) approach has been applied to obtain a more accurate solution of the diffusion equation. The MF approach has been coupled with the static hysteresis and the excess-field models. Then the governing equation has been set to be weakly satisfied to obtain the coefficients of the Fourier series.

The effectiveness and accuracy of the proposed model have been evaluated by comparing the model results with the measurements performed under multi-harmonic sinusoidal flux density waveforms. The comparison reveals that the proposed magneto-dynamic model is able to approximate the magnetic field and iron losses in laminated steels with a relative energy-error of less than 7% for complicated magnetization behavior resulting from an arbitrary flux density waveform.

The objective of this paper is to evaluate the performance of the congruency-based static hysteresis model proposed in [11] when it is coupled with the dynamic field components, i.e. eddy-current and excess fields. The presented results prove that the applied static hysteresis model has a considerable contribution to the achieved accuracy. The main drawback of the congruency-based static hysteresis is that its identification procedure is more difficult than the identification procedure for the other conventional hysteresis models because more measurement data is required.

The high accuracy offered by the congruency-based static hysteresis model makes it a proper choice to be coupled with electromagnetic solvers such as finite element (FE) for accurate iron loss prediction in electromechanical devices. However, the proposed static model is a scalar one and it should be extended to a vector model. For this purpose, the vector generalization proposed by Mayergoyz [20] can be applied to the scalar model. The measured uni-axial FORCs and SORCs are used to obtain the FROCs and SORCs of the vector model by adapting the identification procedure proposed in [20]. The accuracy of the proposed scalar hysteresis model will result in a more accurate vector model, however, due to the large amount of measurement data the identification procedure of the vector model will be more difficult than the identification procedure of other conventional hysteresis models. Extension of the proposed scalar model by the vector generalization will be studied thoroughly in a separate paper.

Author contribution statement

R. Zeinali developed the theoretical formalism, performed the numerical simulations, and carried out the experiments. R. Zeinali wrote the manuscript in consultation with both D. Krop and E. Lomonova authors. D. Krop and E. Lomonova supervised the findings of this work and provided critical feedback and helped shape the research, analysis, and manuscript.

References

1. G. Bertotti, IEEE Trans. Magn. **24**, 621 (1988)
2. E. Dlala, A. Belahcen, A. Arkkio, IEEE Trans. Magn. **46**, 3101 (2010)
3. G. Bramerdorfer, D. Andessner, IEEE Trans. Ind. Electron. **64**, 2530 (2017)
4. G. Bertotti, I. Mayergoyz, in *The Science of Hysteresis: Hysteresis in Materials*, 1st edn. (Academic Press, 2005), Vol. 3
5. M. De Wulf, L. Vandevelde, J. Maes, L. Dupré, J. Melkebeek, IEEE Trans. Magn. **36**, 3141 (2000)
6. O. Henze, W.M. Rucker, IEEE Trans. Magn. **38**, 833 (2002)
7. S. Hussain, D.A. Lowther, IEEE Trans. Magn. **54**, 1 (2018)
8. R. Zeinali, D.C. Krop, E. Lomonova, H.B. Ertan, in *Proceedings - 2018 23rd International Conference on Electrical Machines, ICEM 2018* (2018), pp. 1031–1036
9. S. Steentjes, K. Hameyer, D. Dolinar, M. Petrun, IEEE Trans. Ind. Electron. **64**, 2511 (2017)
10. S.E. Zirka, Y.I. Moroz, P. Marketos, A.J. Moses, IEEE Trans. Magn. **40**, 390 (2004)
11. R. Zeinali, D.C.J. Krop, E.A. Lomonova, IEEE Trans. Magn. **56**, 1 (2020)
12. I.D. Mayergoyz, *Nonlinear Diffusion of Electromagnetic Fields: With Applications to Eddy Currents and Superconductivity* (Elsevier, 1998)
13. S.E. Zirka, Y.I. Moroz, P. Marketos, A.J. Moses, IEEE Trans. Magn. **42**, 2121 (2006)
14. O. Bottauscio, A. Manzin, A. Canova, M. Chiampi, G. Gruosso, M. Repetto, IEEE Trans. Magn. **40**, 1322 (2004)
15. M. Petrun, S. Steentjes, K. Hameyer, D. Dolinar, IEEE Trans. Magn. **52**, 1 (2015)
16. V. Podlogar, B. Klopcic, G. Stumberger, D. Dolinar, IEEE Trans. Magn. **46**, 602 (2010)
17. S. Hamada, F.Z. Louai, N. Nait-Said, A. Benabou, J. Magn. Magn. Mater. **410**, 137 (2016)
18. J. Gyselinck, R.V. Sabariego, P. Dular, IEEE Trans. Magn. **42**, 763 (2006)
19. P. Rasilo, E. Dlala, K. Fonteyn, J. Pippuri, A. Belahcen, A. Arkkio, IET Electric Power Appl. **5**, 580 (2011)
20. I.D. Mayergoyz, J. Appl. Phys. **8**, 4829 (1991)

Cite this article as: Reza Zeinali, Dave Krop, Elena Lomonova, Modeling the dynamic behavior of laminated steels using a Fourier-based approach, Eur. Phys. J. Appl. Phys. **92**, 10905 (2020)